A Hyper-Spectral Multi-Sensor Infrared Radiance Data Record for Climate Trending: Validation using Simultaneous Nadir Observations

March 2, 2016

Contents

1 Abstract.

The need for long term climate data records from space-borne measurements places stringent requirements on sensor calibration stability and of continuity between different sensors. Pre-launch and in-flight calibration methods have improved over recent generations of sensors, which have helped reduce the absolute uncertainty, as demonstrated through inter-comparison studies between sensors and independent data records. In the case of hyperspectral infra-red sensors knowledge of the accuracy of the radiance measurement as a function of frequency is of fundamental importance. When two sensors are operational at the same time and provide a period of overlap then the bias characteristics of radiance measurements can be determined. In this paper we evaluate the bias between three similar sensors that have multiple year overlap using simultaneous nadir overpass observations. We report on the techniques used to determine the radiance bias for the many channels over the spectral range of the sensors, in which the spectral content of each channel is matched to a common grid. This is especially important at wavelengths of high contrasting emission lines. The quantitative methods to translate the spectral response functions of different spectrometers and the line shapes of different interferometers to a common spectral grid are described. We report on results of comparison of sensor bias over the spectral range common to all sensors and the merging of measurements to create a common radiance record which is suitable for climate trending research. The large number of simultaneous nadir observations that are available provide statistically significant measurements of bias between the sensors. We evaluate clearly traceable uncertainties to the final estimates from which a common radiance record is derived. Over much of the spectral and dynamic range of the sensors studied this method resolves sensor bias to the order of 10 mK with sensor bias of order 0.2 K, which is a function of the frequency.

2 Introduction

Detection of climate change signals requires long-term, highly accurate measurements with optimal spatial coverage, for example [1] The time period needs to be longer (nominally twice longer) than the longest period of variability of interest. The accuracy implies absolute calibration stability with low and well characterized measurement noise and spectral stability. The spatio-temporal resolution and coverage needs to accurately represent the true state over the whole globe and be sufficient to resolve extremes of nat-

ural variability. The last requirement is particularly hard to achieve with ground based observations, and so global observations from space are better able to provide such spatial coverage.

The time period of interest is largely determined by the current knowledge of the climate system as it is influenced by natural internal variability and by it's response to external forcing, including human induced environmental changes. Those of longest periodicity of interest in this context include, but are not limited to, the El Nino Southern Oscillation (ENSO), the Pacific Decadal Oscillation (PDO) and Atlantic multi-decadal oscillation (AMOC), and external factors such as impacts of human activities and industrial processes. See for example, the IPCC (Intergovernmental Panel on Climate Change) assessment report 4, working group 1 and references therein [2]

The measurements that are made of various climate and environmental variables (ECVs) as defined, for example, by the World Meteorological Organisation (WMO) Global Climate Observing System (GCOS) need to have sufficient dynamic range, resolution and absolute calibration accuracy to properly record the variable being measured and be capable of distinguishing small climate signals or trends from the short period large apmlitude variations. These are qualitatively delineated on the WMO GCOS web site, reference [3].

The spatial sampling of the measurements, needs to be sufficient so that any one measurement be representative of the area (or volume) in which it is taken and that all areas of the world are equally represented. This can be an issue between adjacent high contrast scenes such as land/ocean boundaries, deep convective clouds, for example.

There are a large variety and number of sensors being used to measure the ECVs, and new ones are deployed to augment or replace old sensors. This is true of satellite sensors, where calibration trending is more challenging than earth-based sensors. Early generations of satellite sensors had relatively short operational lifetimes, their absolute calibration less well known and the succeeding sensors were different which meant detection of climate signals was very difficult. Since around the 1990s improved technologies have resulted in more stable sensors and longer periods of observations with the same sensor, furthermore, new ones have been deployed so there is a substantial overlap. This helps to produce a meaningful climate quality data record. Nevertheless, the sensors and the observational sampling are not identical, and so it is necessary to develop new techniques to analyze and merge the data sets to obtain a product that can be used toward climate research.

This paper is concerned with a method for producing a continuous cli-

mate data record in radiance units from the hyper-spectral infra-red measurements obtained from low-Earth orbiting (LEO) satellites by merging the radiance observations on to a common wavenumber scale.

The following sections first describe the sensors and observations available to us; then the method for translating the observations to a common frequency scale; then the validation of the methods using SNO pairs with a discussion of results, conclusions and suggested further work.

3 Observations

The sensors used in this study are the Atmospheric InfraRed Sounder (AIRS) on the NASA EOS Aqua satellite, the Cross-track Infrared Sounder (CrIS) on the Suomi-NPP satellite and the Infrared Atmospheric Sounding Interferometer (IASI) on the European Metop satellite.

In brief summary, AIRS is an echelle grating spectrometer covering the spectral range from 3.74 to 4.61 μm , from 6.20 to 8.22 μm, and from 8.8 to 15.4 μm, with nominal spectral resolution $\lambda/\delta\lambda = 1200$ using a total of 2378 spectral channels. The details of the spectral response functions are publically available e.g see reference [4]. AIRS is mounted on the NASA EOS Aqua spacecraft which is in a LEO sun-synchronous orbit with 98 degree inclination and equator crossing about 1:30pm. AIRS is a nadir sounder with a lateral scanning mirror that provides 90 footprints from about 45 degree either side of nadir. The footprints are about 13.5 km diameter at nadir. For more details see reference [5]. The data used for this work are the level 1b geolocated calibrated radiances, which are further processed to level 1c for conversion, see below.

The CrIS sensor is a Michelson interferometer with 1305 channels covering the spectral range in three sub-bands from 3.92 to 4.64 μ $m, 5.71 to 8.26 μm and 9.13 to 15.3 μm . When first launched, the spectral resolution in each sub-band was different with LW: 0.625 cm^{-1}, MW: 1.25 cm^{-1}, SW: 2.5 cm^{-1}, but since December 2014 all bands operate with 0.625 cm^{-1} resolution. CrIS is mounted on the Suomi-NPP weather satellite, also in a LEO, sun-synchronous, 98-degree inclination orbit and 1:30 pm equator crossing time. The Suomi-NPP orbit altitude is about 100 km higher than AQUA, so it's orbit period is slightly longer. CRiS is a nadir sounder with a lateral scanning mirror that provides 30 ground views within 45 degrees either side of nadir. Each ground view consists of nine fields of view on a square grid, each with a diameter 14 km at nadir. For more details see for example references [6] and [7]. The data used in this work are the geolocated calibrated

radiances processed through the IDPS system.

The IASI sensor is a Michelson interferometer with 8461 channels covering the spectral range from 3.62 to 15.5 μm with a nominal resolution of about 0.5 cm^{-1}. IASI is mounted on the MetOp satellite, also a LEO, sun-synchronous, 98 degree inclination, with a 9:30 am equator crossing time. IASI is a nadir sounder with a lateral scanner. Each ground view consists of four fields of view on a square grid, each 13 km diameter at nadir. There are 30 ground views within 45 degrees either side of nadir. For more details see for example references [8] and [9]. The data used are the gelocated calibrated radiances supplied to level 1c.

AIRS has been operating since about June 2002, CRIS on Suomi-NPP since about December 2011 and IASI-1 on MetOp-A since about November 2006 and IASI-2 on Metop-B since about October 2012. There is therefore considerable temporal overlap of these missions for which comparisons can be made. At the time of writing CRIS-2 on JPSS-1 is due for launch early 2017. Note that the orbit of Metop-A has morning equator crossing whilst AQUA and Suomi-NPP and afternoon crossing which influences where the SNOs are located.

It is worth noting that there have been continuous hyperspectral infrared global atmospheric soundings since 2002, and the prospect of another decade or so with just those instruments described above. Furthermore, the spectral range, spectral resolution and spatial sampling of these sensors have similar attributes, which permits comparisons to be made rather readily. Nevertheless, differences between the sensors must be accounted for correctly.

With the relatively long and increasing data set, it is possible to relate the observations to known components of global internal climate variability and average global warming trends. There are several possible ways this can be done, including tracking levels of long-lived (passive) tracer gases, cloud amounts and surface temperature.

In this paper we describe the direct comparison of spectral radiance at the top of the atmosphere (TOA) as measured by the sensors. We produce a TOA spectral radiance data set with a common spectral grid and equivalent spectral response that can be used with multiple sensors to support climate studies.

The techniques used and their validation are presented in the following sections.

4 Method

This section describes the techniques and methods used to generate a common set of spectral radiance channels from the individual sensors. The choice of a spectral scale, or grid, that is common to multiple sensors, is made considering which contains as much of the spectral range of overlap of all sensors and is the lowest resolution. In practice the resolution of all sensors is not much different, so the choice to use CrIS standard resolution is convenient. In theory, any real or synthetic grid could be used. This choice may be revisited in the future, since CrIS changed to high-resolution in all three of its bands in December 2014.

Consider the case in which the spectral radiance received at the sensor is a very well known, slowly varying function of frequency, as for a blackbody Planck emitter. Then for a variety of sensors with different spectral response functions (SRF) or instrument line shapes (ILS) one could choose a subset of channels that include the spectral range of all sensors. This subset could be chosen from one of the sensors or be synthesized. In general the spectral resolution of this common subset would not be finer than the widest of the sensors, however, in practice this need not be a constraint.

Given knowledge of the variation of the actual spectral radiance at the sensors, which in this case is a very well known Planck function, then the radiance can be evaluated at a finer spectral grid than the sensor resolution, which is effectively de-convolving the monochromatic radiance from the instrument response. The accuracy to which this can be done will be limited by the knowledge of the SRFs and the approximation due to the choice of the fine working grid. In this work, the pseudo-monochromatic radiance is determined at 0.0025 cm^{-1}, the AIRS SRFs are evaluated at 0.01 cm^{-1} resolution and the intermediate grid is 0.1 cm^{-1}.

In the more realistic case of actual TOA radiance across the infrared bands, the spectra radiance is only approximately known by the sensor, given the resolution of its SRFs or ILS and detector noise. The deconvolution to the intermediate grid will similarly be an approximation and the degree to which this is the case depends upon how well the radiance signal is spectrally resolved by the sensor. This is self-evident if there are gaps between SRFs (in the case of a spectrometer), or if the SRF or ILS is broad compared to an emission line, for example. The method works well because there is spectral information contained several wavenumbers beyond the nominal width of each sensor channel.

Suppose there are n channels on a frequency grid v of k points spanning the domains of the functions srf_i . Let S_k be an $n \times k$ array such that

$s_{i,j} = srf_i(v_j)/w_i$, where $w_i = \sum_j srf_i(v_j)$, that is where row i is $srf_i(v)$ tabulated at the grid v and normalized so the row sum is 1. If the channel centers are in increasing order S_k is banded, and if they are not too close, the rows are linearly independent. S_k is a linear transform whose domain is radiance at the grid v and whose range is channel radiances. If r is radiance at the grid v, then $c = S_k r$ gives a good approximation of the channel radiances $c_i = \int srf_i(v) r(v)\, dv$.

Considering the AIRS sensor, with the deconvolution applied to the intermediate grid, at 0.1 cm^{-1} , and let $v_b = v_1, v_2, \ldots, v_m$ at the resolution of the tabulated SRFs. Similar to S_k, let S_b be an $n \times m$ array where row i is $srf_i(v)$ tabulated at the v_m grid, with rows normalized to 1. If r is radiance at the grid v_b, then $c = S_b r$ is still an approximation of $\int srf_i(v) r(v)\, dv$, since in practice it is performed on a discretized grid.

Consider the linear system $S_b x = c$, similar to the case $S_k x = c$ above, where we are given S_b and channel signals c and want to find radiances x. Since $n < m < k$, as with S_k, the system will be under-determined, but more manageable because for the default resolutions m is approximately 40 times less than k, so finding the pseudo-inverse of S_b becomes tractable.

The AIRS L1b data are pre-conditioned using routines to clean up the noisy channels, fill gaps with simulated radiance and trim for acceptable channel spacing, then the matrix S_b is much improved with a condition number around 30.

The deconvolved radiance on the intermediate grid is next reconvolved onto the CRIS user grid by double Fourier transformation. The useful channels are those that are included in the intersection of the bands of both sensors. This process allows direct comparison of radiance between AIRS and CRIS for the CRIS spectral channel positions. Only those channels that were not altered by the AIRS L1b clean and fill routine are used for comparison.

The IASI to CrIS is a relatively easy translation because the IASI instrument spans the CrIS bands and has a nominal (though strongly apodized) higher resolution. Furthermore, IASI, unlike AIRS does not require preconditioning of any channels. For this translation, the IASI frequency grid is interpolated to the intermediate grid (0.1 cm^{-1} TBC), then the radiance is converted to the interferogram with the Fourier transform, to which is applied the inverse IASI apodization which is then taken back to radiance. This is then convolved from the intermediate grid to the CRIS channels. As would be expected, some ringing occurs at the band edges.

5 Validation

The translation of AIRS and IASI to the CrIS spectral grid is validated primarily by simulating the TOA radiance at high spectral resolution then convolving with the instrument SRF or ILS, then passing the simulated sensor signals through the translation process as outlined in the previous section and comparing results. For convenience, the full infrared spectral range from about 645 cm^{-1} to 2570 cm^{-1} is divided into three sub-regions labelled long, medium and short (LW, MW and SW).

The simulated TOA radiance is produced using the UMBC k-Compressed Radiative Transfer Algorithm (kCARTA) line-by-line (LBL) model and 49 standard atmospheric composition profiles. The forward model is computed at the native resolution of 0.0025 cm^{-1} and then convolved with the instrument response functions to produce a simulated true spectral radiance signal as measured by the sensors. The AIRS spectra are then translated onto the CrIS spectral grid, referred to as AIRS-to-CrIS, and the two are compared by simple subtraction. The average difference and the standard deviation are evaluated and plotted. The same is done for IASI-to-CrIS. Figures 1 shows the LW band brightness temperature spectrum for the translation AIRS to CrIS.

The main points to note are as follows. For the AIRS and CrIS differences, the L1C channel set for AIRS is used. This uses 2645 channels, and fills the gaps of the L1b set so as to create a uniform channel set for the deconvolution. The first couple of channels at the longwave end at 645 cm^{-1} and shotwave end at 1610 cm^{-1} are dominated by band edge effects. For most of the region from 650 to 1610 cm^{-1} the

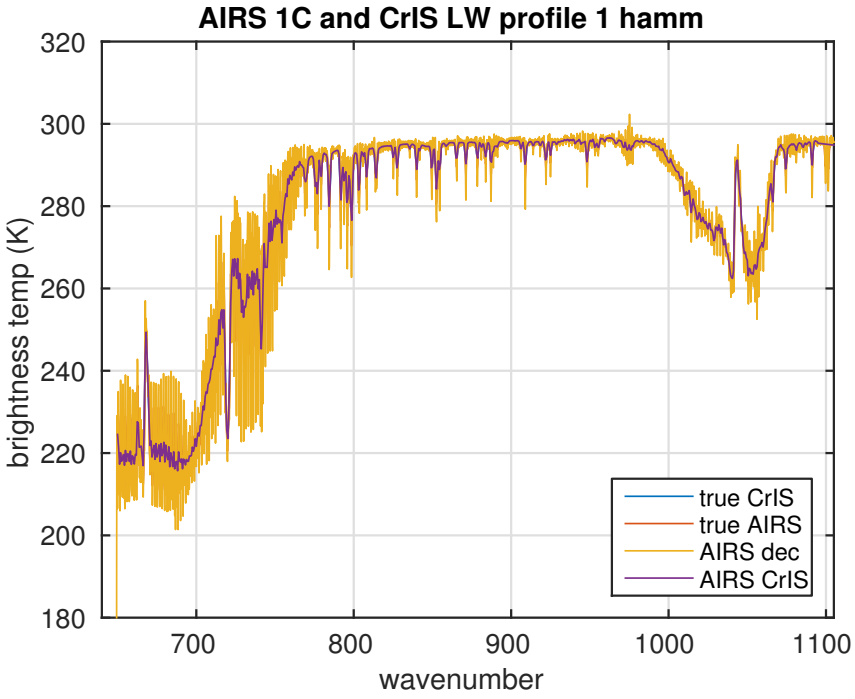

Figure 1: Brightness temperature spectra for AIRS to CrIS LW band.

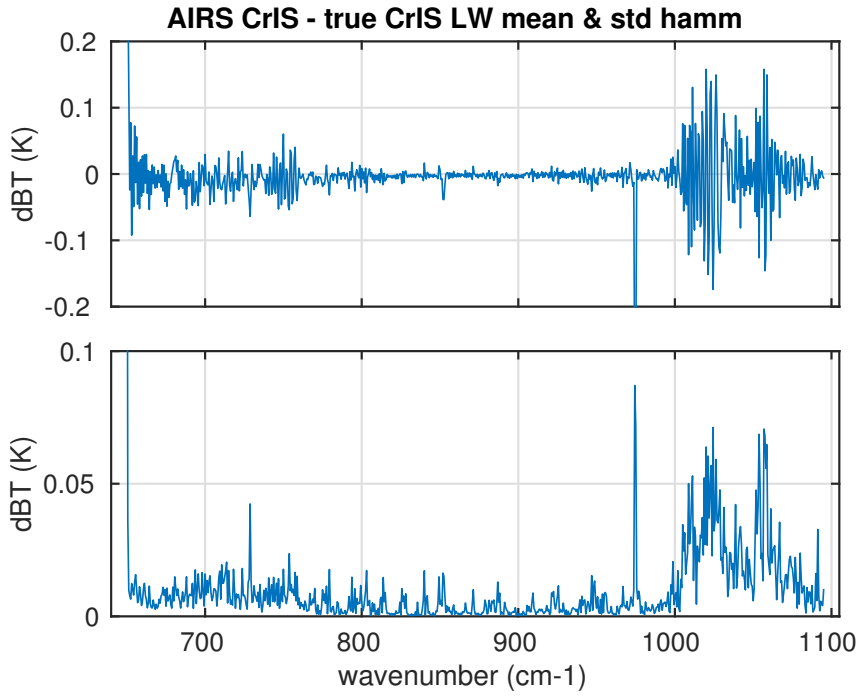

Figure 2: BT bias and standard deviation for AIRS to CrIS LW band.

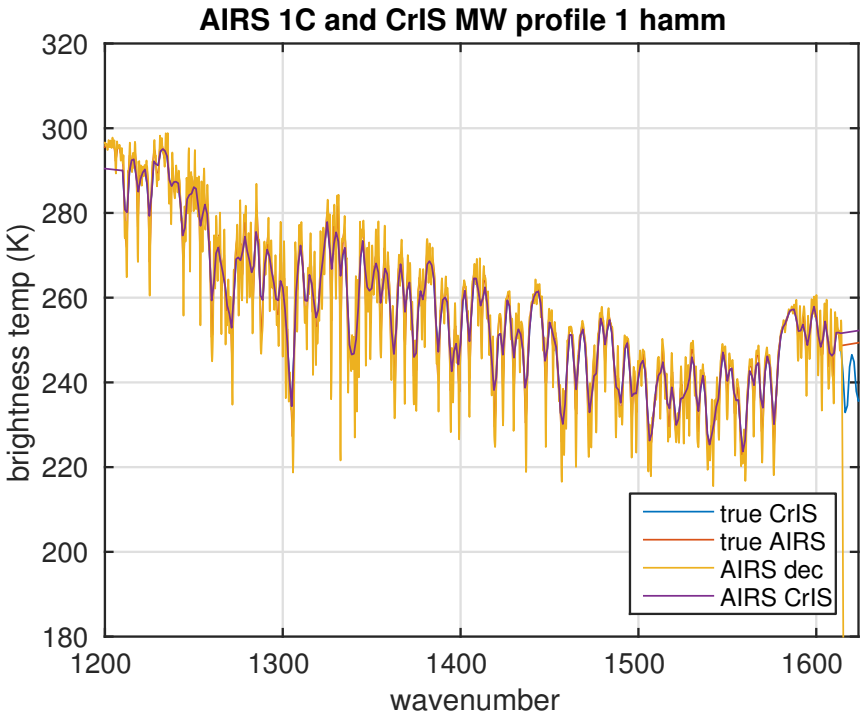

Figure 3: Brightness temperature spectra for AIRS to CrIS MW band

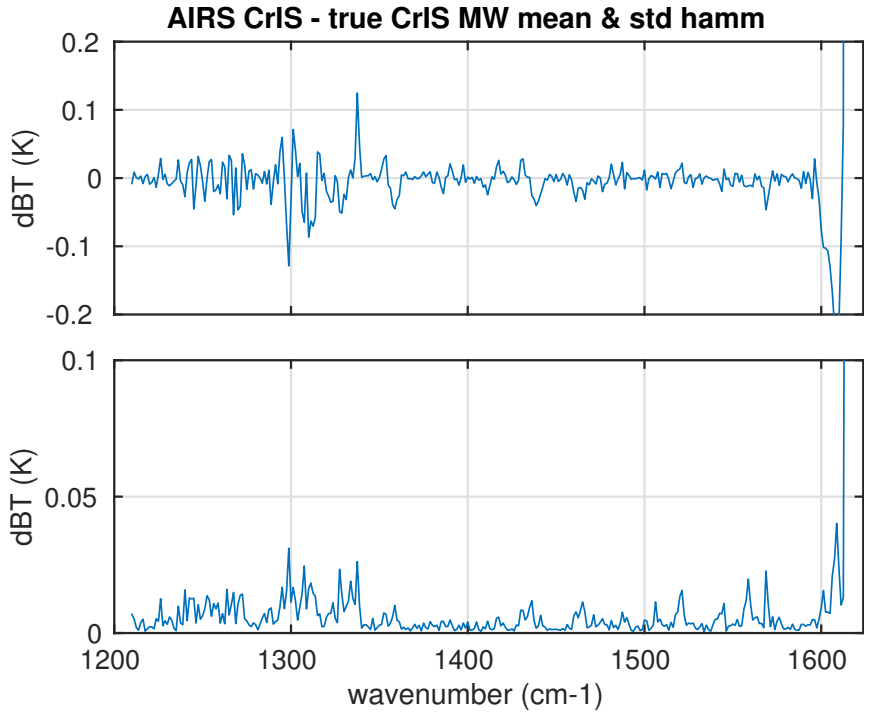

Figure 4: BT bias and standard deviation for AIRS to CrIS MW band.

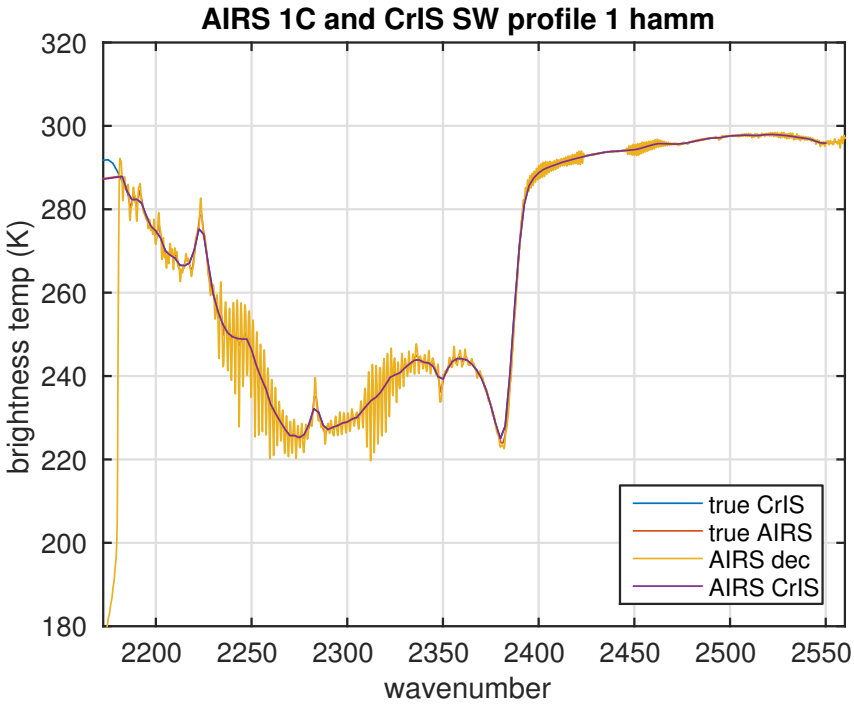

Figure 5: Brightness temperature spectra for AIRS to CrIS SW band.

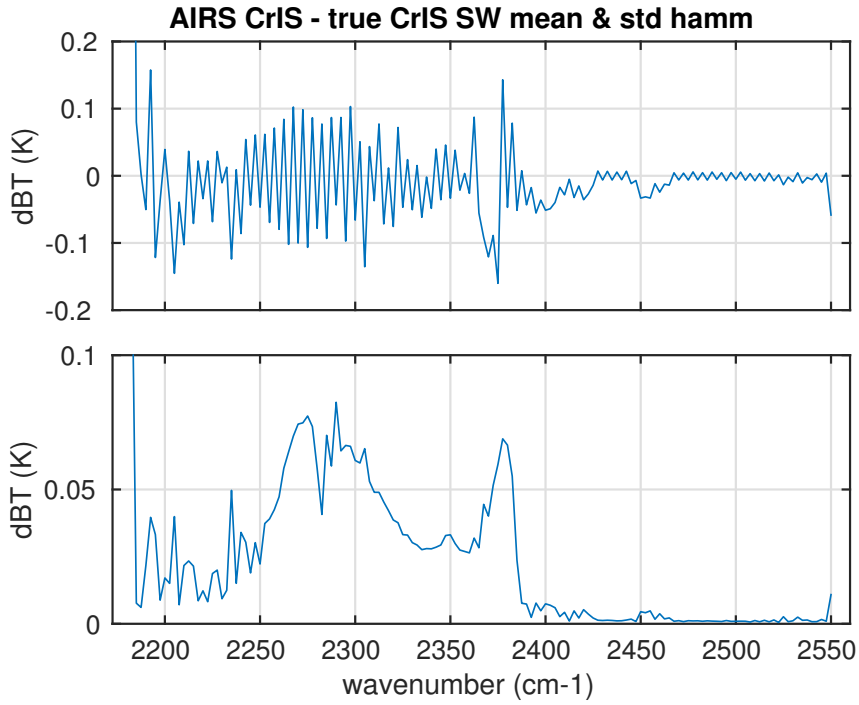

Figure 6: BT bias and standard deviation for AIRS to CrIS SW band.

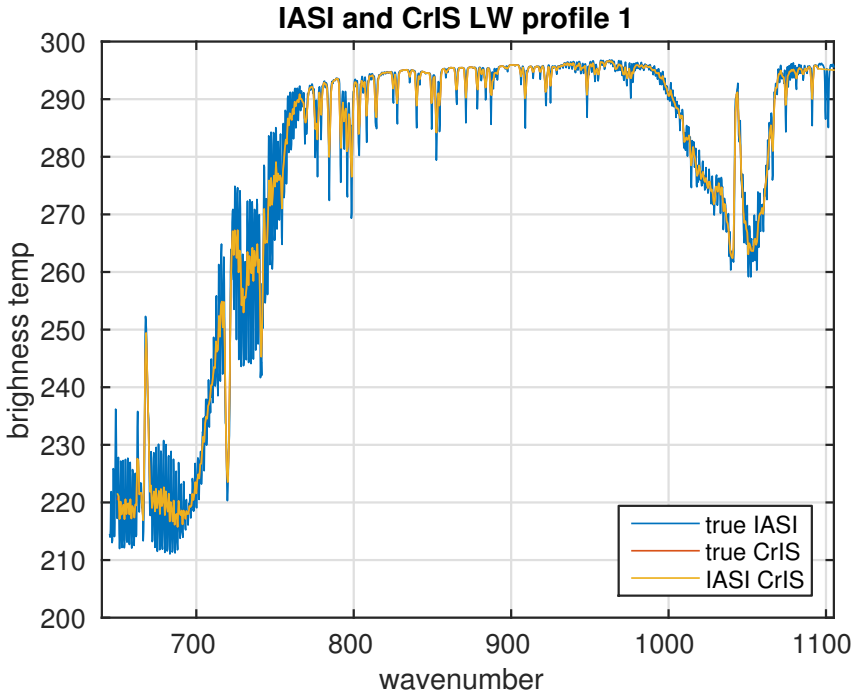

Figure 7: Brightness temperature spectra for IASI to CrIS LW band.

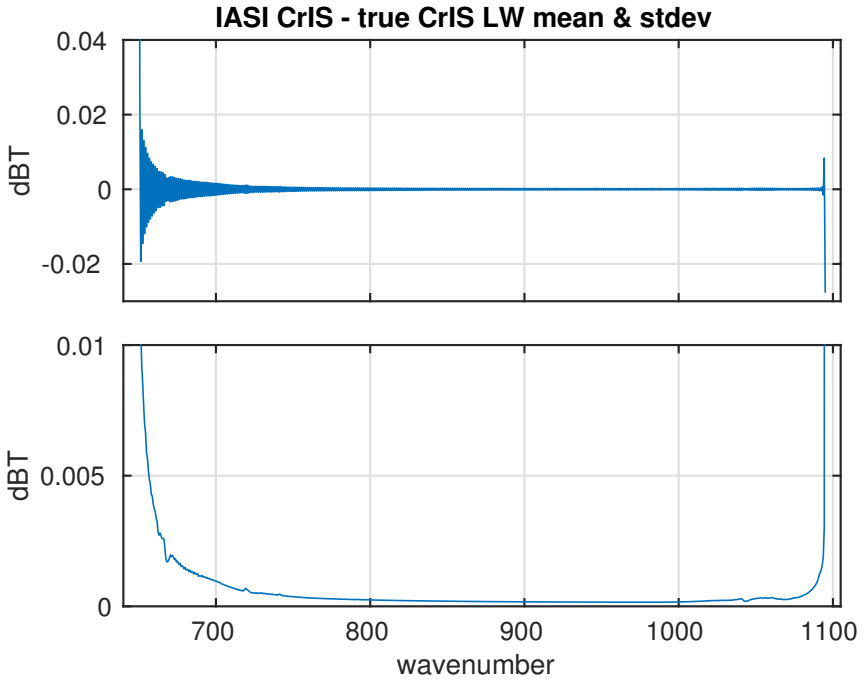

Figure 8: BT bias and standard deviation for IASI to CrIS LW band.

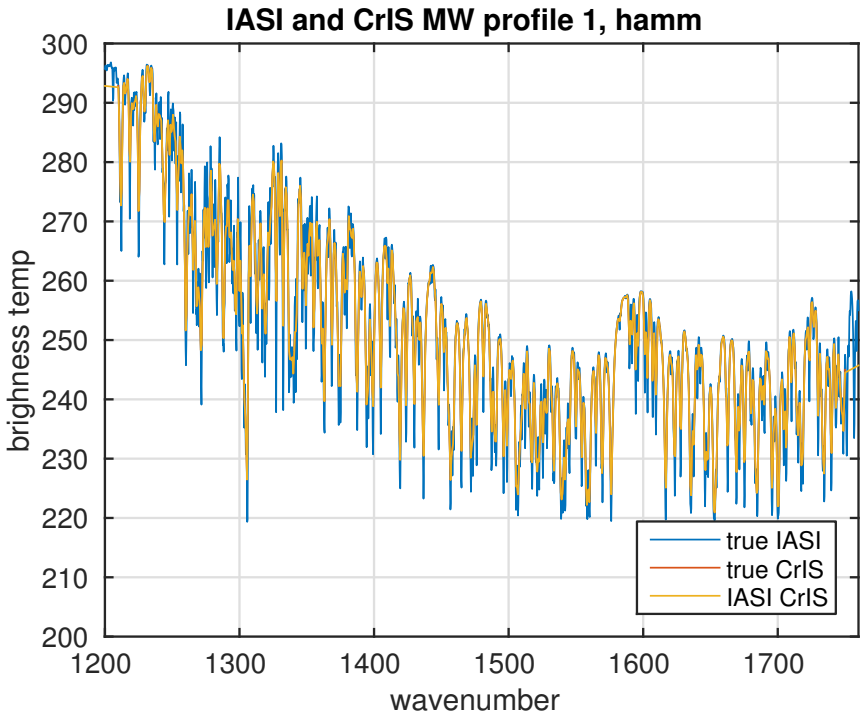

Figure 9: Brightness temperature spectra for IASI to CrIS MW band.

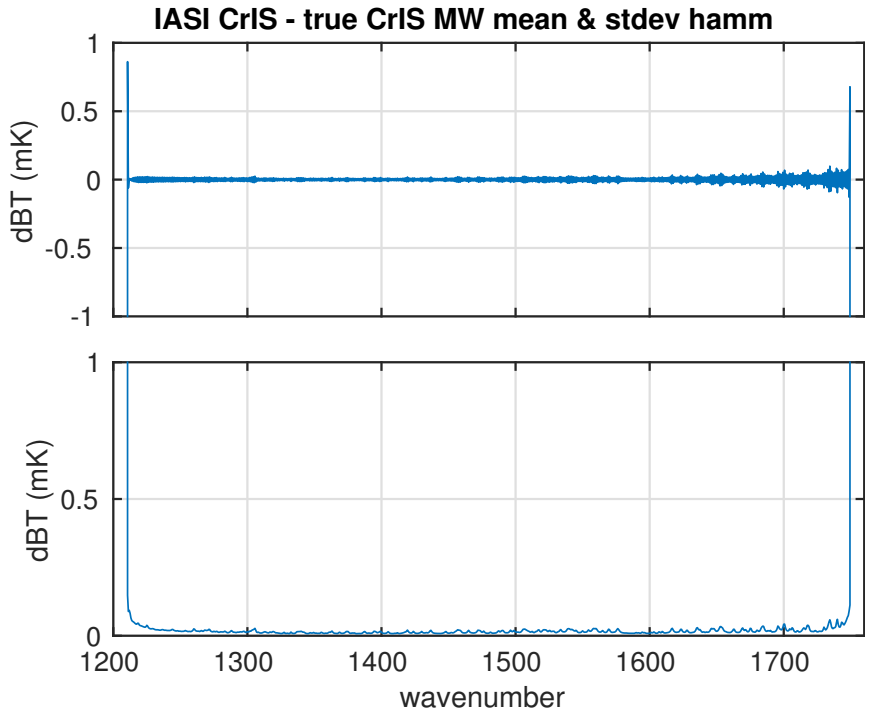

Figure 10: BT bias and standard deviation for IASI to CrIS MW band.

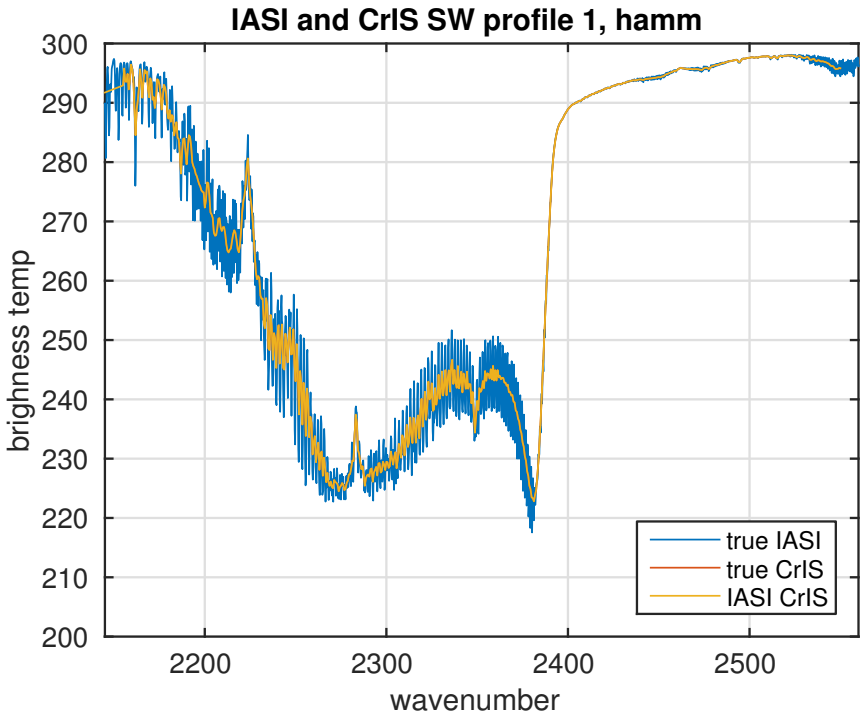

Figure 11: Brightness temperature spectra for IASI to CrIS SW band.

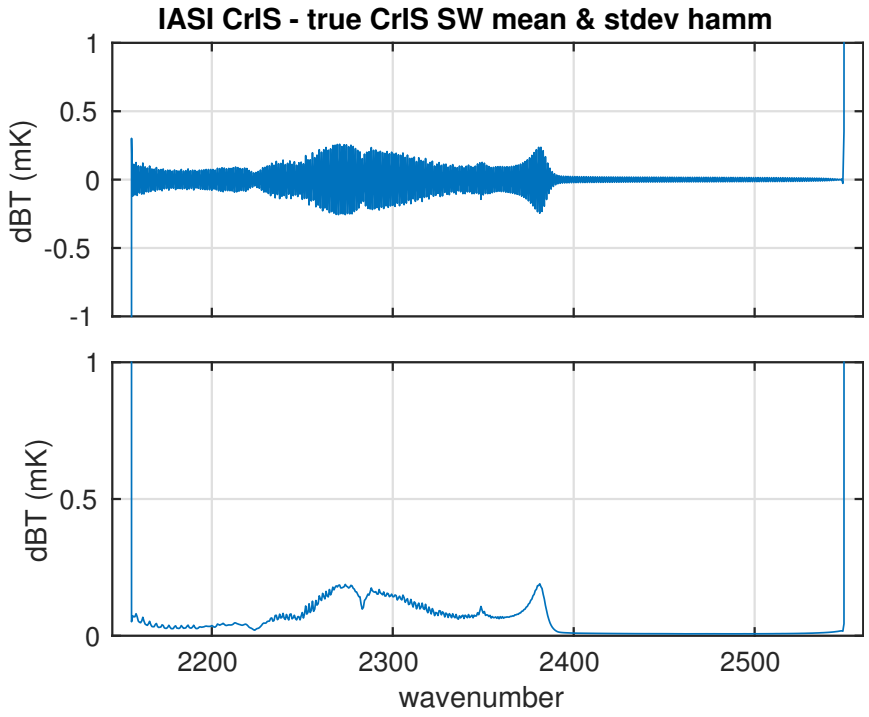

Figure 12: BT bias and standard deviation for IASI to CrIS SW band.

6 Results

The following sub-sections summarize some of the main attributes of the bias between each pair of sensors, each as a function of wavenumber and in some cases also as a function of the dynamic range of selected spectral channels. For the IASI and CrIS set the IASI spectral radiances are converted to the CrIS grid; for the AIRS and CrIS set the AIRS are converted to the CrIS grid; and for the AIRS and IASI set, the IASI are converted to the AIRS grid. In the fourth sub-section, a summary is provided with AIRS and IASI sets each plotted on the CrIS grid, as it is from this result that the common climate radiance record is to be constructed. In this study, we do not consider the shortest wavelength channels that are affected by reflected solar radaition.

6.1 IASI and CrIS SNOs

The selection criteria for the IASI and CrIS SNOs are that any of the field of views (FOV) for the field of regards (FOR), sometimes called foot-print, numbers 15 and 16, for each sensor are within 13 km and 20 minutes of each other. Note that IASI has four simultaneous FOVs per FOR and CrIS has 9 simultaneous FOVs per FOR. For each SNO pairing the FOVs are recorded.

The data set used here encompass the period from April 2012 to February 2014, in which there are 275,511 SNO pairs. Because of the different orbits of Suomi-NPP and Metop-A the coincident observations only occur at high latitudes as shown in figure 13

Since the latitude range is very limited, the variation of time delay and separation of each sensor pair is unremarkable. However, because the location of the samples is at hight latitudes there will be few very warm surface observations, and the solar zenith angle is large (near and above 90 degrees). Furthermore, there will be high sensitivity to scene inhomogeneity, with land/sea ice and ocean contrasts in close proximity, at least in the window channels. By way of example, the range and distribution of the brightness temperature in the 899 cm^{-1} window channel is shown in figure 14 for all practical purposes, the maximum range of B.T. observed by CrIS is from about 180 K and 310 K respectively. Clearly, the majority of scenes involve ice - either in cloud or on the ground.

Evaluation of the bias between the two sensors is achieved by first converting all the IASI spectra on to the CrIS spectral grid, using the deconvolution tool described above. In the following figure 15 the average difference of all SNO pairs is evaluated, together with the standard error of the mean difference. A very few observations are eliminated based on the IASI quality

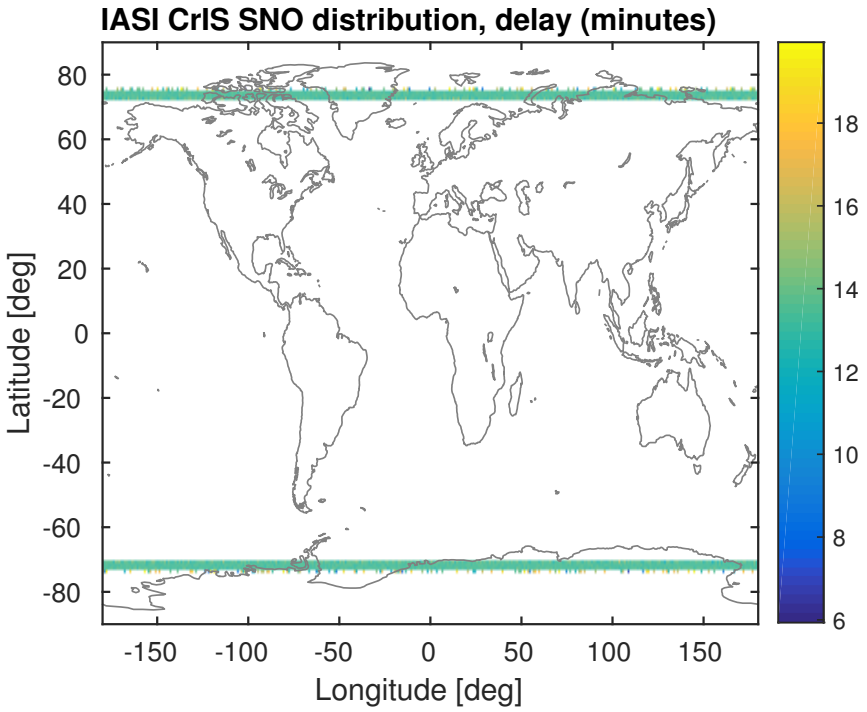

Figure 13: Location map of IASI CrIS SNOs, with time delay in minutes.

flag. Notice the general slope in bias from 0.2 K to about 0.5 K from the long-wave to short wave end. The large bias of the first two or three channels at the ends of this band reflect the band edge limit of the deconvolution, and are not used.

It is necessary to examine more closely the characteristics of the bias with this data set because of the highly restricted spatial coverage, and potential sampling differences between the north and south regions. For this purpose the SNO set is divided into two separate subsets, one based on whether the scenes are in day-time or night-time, and one based on whether they are in the north or south polar regions. Figure 16 show the mean spectrum for the LW for IASI and CrIS and the bias separated by day/night observations. Also shown is the standard error of the bias in each subset. Notice, that despite the large difference in the mean brightness temperatures, the biases are within error the same.

Figure 17 shows the mean spectrum for the LW for IASI and CrIS and the bias subset into north and south regions, also shown is the standard error of the mean bias. As with the day/night subset although the scenes are very

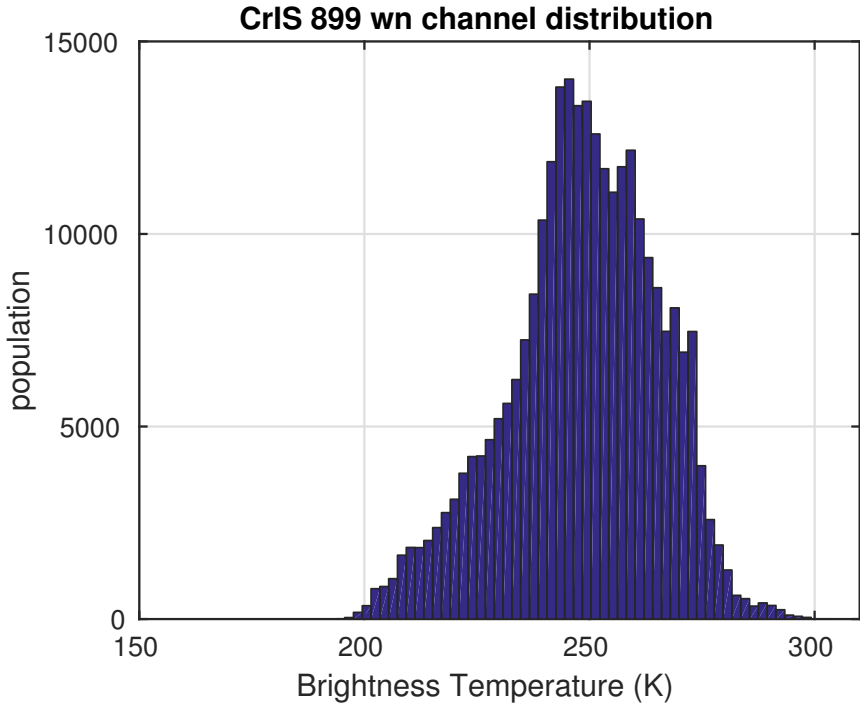

Figure 14: CrIS window channel brightness temperature distribution of the samples.

different the mean biases are negligibly different.

To determine if the bias is independent of the dynamic range, the SNO pairs are binned according to the brightness temperature as seen by each sensor in each channel from each pair. It is important to include the contribution from each sensor in each brightness temperature bin without duplication to ensure that there is no artifact of sampling. In other words, for each SNO pair for a given channel, test whether the CrIS observation falls into a given brightness temperature bin regardless of the IASI observation, then repeat the selection based upon the IASI observation regardless of the CrIS observation, eliminating any repeated samples. A fine-grained quantile profiler is used to select the bin values for each channel, since different wavelengths will see different dynamic ranges. In dividing up the samples into small bins care must be taken to consider the sample statistics, in particular the sample size and the standard error of the bias. As can be seen from figure 18 the sample size per bin becomes very small at the hot and cold extremes of the range and the standard error grows large there as well. Note that in this

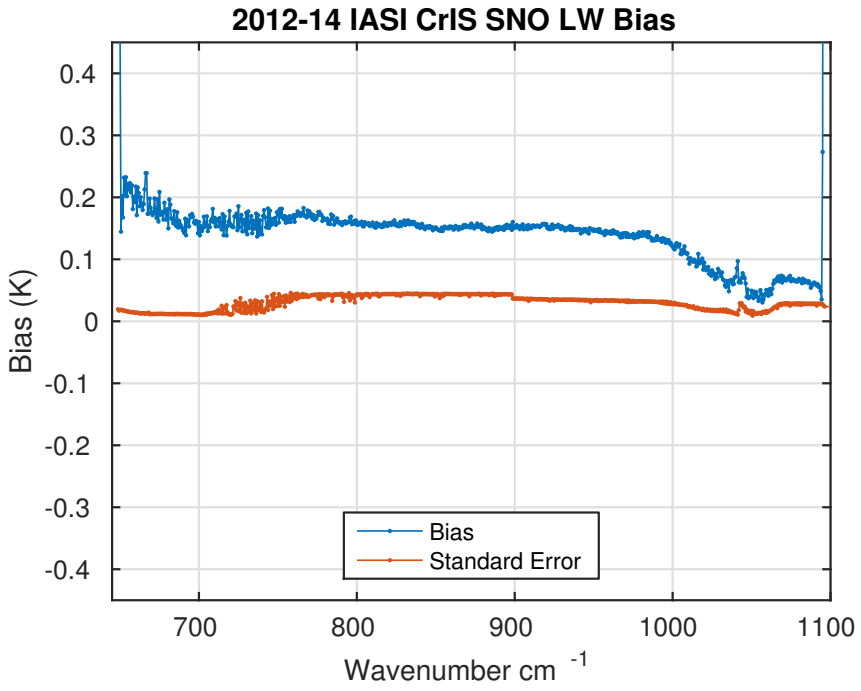

Figure 15: CrIS - IASI bias (K) for all SNO samples from the set, in the LW band.

plot the bias is the IASI minus the CrIS observation, and compare the value at $900cm^{-1}$ to that shown in figure 15 . Examining this figure suggests that the bias is less, and rather close to zero near 270 K, and increases slightly to colder scenes, with CrIS observations warmer than IASI. The limit of the sampling is from about 210 K to 280 K scenes, outside this range the bias result is unreliable.

Taking all 160 channels from about 800 *to* $900cm^{-1}$, the bias variation with scene is very consistent, with no outliers, summarizing these in figure 19 showing the mean bias and standard deviation for all 160 channels. Taking small groups of channels starting at the longest wavelength (lowest numbered) shows the the bias is more constant with scene temperature and from about 710 cm^{-1} the bias takes on a slope like that shown in figure 19 . At this point it would be speculation to attribute the variation of bias as a function of radiance, as it could be due to non-linearity of either or both sensors of either polarity.

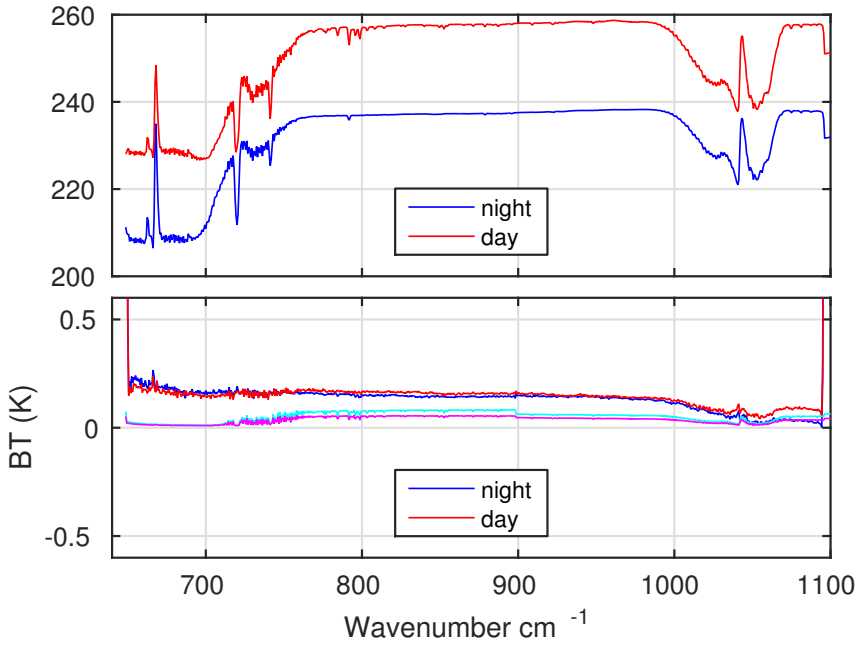

Figure 16: CrIS - IASI bias (K) subset by day and night. Upper panel shows the mean brightness temperature spectrum. Lower panel the mean bias (blue and red) and standard error of the bias (cyan and magenta) for each of the day/night subsets.

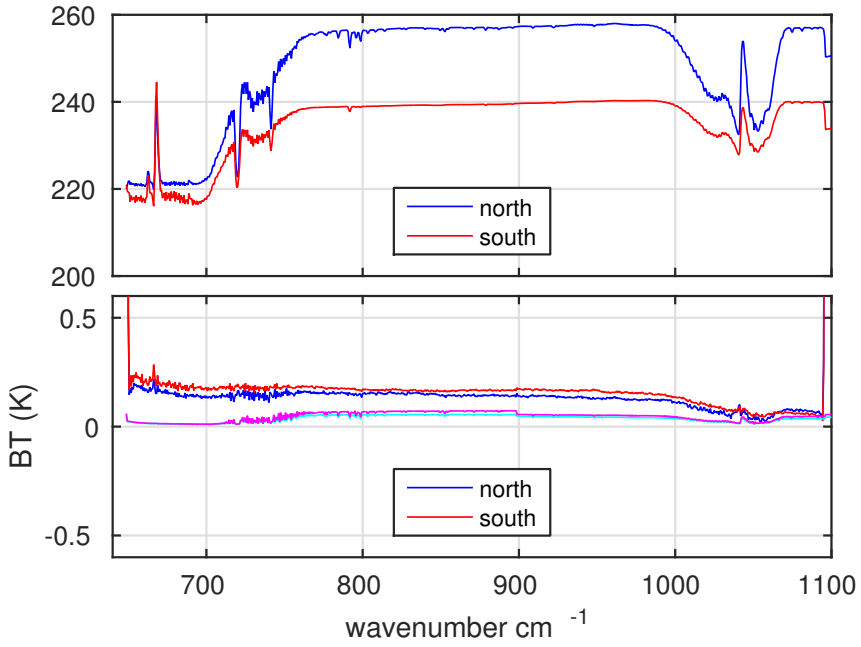

Figure 17: CrIS - IASI bias (K) subset by north and south. Upper panel shows the mean brightness temperature spectrum. Lower panel the mean bias (blue and red) and standard error of the bias (cyan and magenta) for each of the north/south subsets.

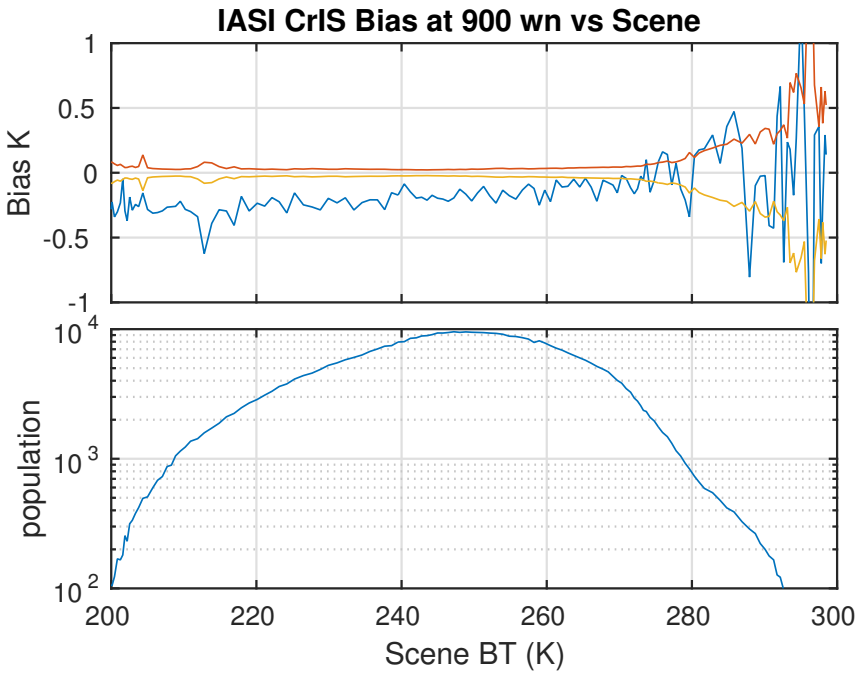

Figure 18: IASI - CrIS bias (K) for channel at 900 cm^{-1} as a function of scene brightness temperature, upper panel, together with the standard error. Lower panel shows the sample size in the bins.

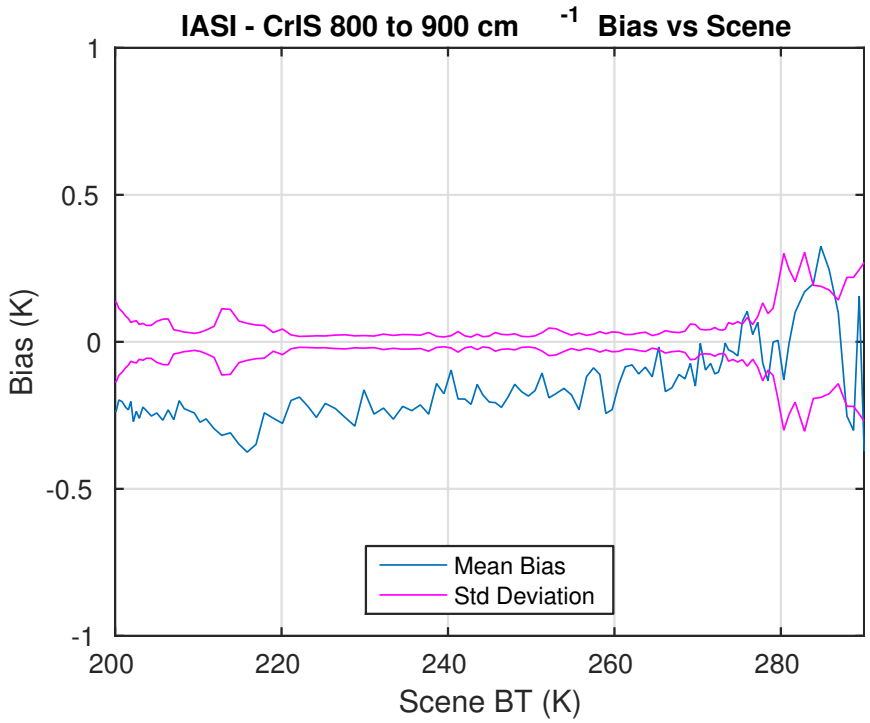

Figure 19: IASI - CrIS bias (K) for all 160 channels from 800 to 900 cm^{-1} as a function of scene brightness temperature, upper panel, together with the standard error.

6.2 AIRS and CrIS SNOs

The selection criteria of the AIRS and CrIS SNOs are that the AIRS FORs numbers 43:1:48, which include 3 fields either side of nadir, and that any of the 9 FOVs in the CrIS FORs 15 and 16 (centered on nadir), are located within 13 km and within 20 minutes of each other for the tropical subset and 10 minutes for the standard set. For each SNO pair the CrIS FOV is recorded.

The data sets used are designated either tropical v10.0.0, or standard at all available latitudes and encompass the calendar year 2013. For the tropical v10.0.0 set there are 4.232 x10^6 SNO pairs, distributed within 50 degrees latitude of the equator. For the 'standard' JPL set there are 1.393x10^6 pairs in 2013, and distributed as shown in figure 20. Note i) there is a much higher density of data near the poles; ii) nearer the equator all pairs have a positive time delay, greatest at the equator with AIRS samples later than CrIS. Since the ascending node is at 1:30 pm local the AIRS samples are later after local solar noon than the CrIS samples during the day; iii) only descending orbit (night) samples are available over Africa and Australia and only day time ones over South America, this has significant impact on the hot bias of the samples. Also note that even with close spatio-temporal sampling, the estimate of bias between the sensors will be better where the scene is more uniform.

It is instructive to examine the distribution and dynamic range of the sample population as a function of brightness temperature, which is best illustrated with a window channel. The 900 cm^{-1} AIRS channel for the standard SNO set is shown in figure 21. Note; i) the distribution is highly non-Gaussian, with a more uniform cold tail and truncated hot tail; ii) The hottest scenes, greater than about 303 are exclusively over land during the day, with a very few up to 331 K; iii) the peak around 295 K is indicative of clear tropical ocean scenes; iv) the peak around 270 is probably freezing water; v) the relatively large population from about 240K to 260 K is due to the large number of cold polar scenes and cold clouds. This can be compared to figure 22 that shows the same information for samples restricted to less than 50 degrees of latitude.

The distribution of sampling delays between the two sensors is also worth noting, as shown in figure 23, with the left panel showing the v10.0.0 tropical set and the right panel the standard, all latitude set.

Of further note is that for channels that are at wavelengths with weighting functions that peak higher in the atmosphere, the distributions tend to be much more Gaussian-like (although not Gaussian) compared to the window

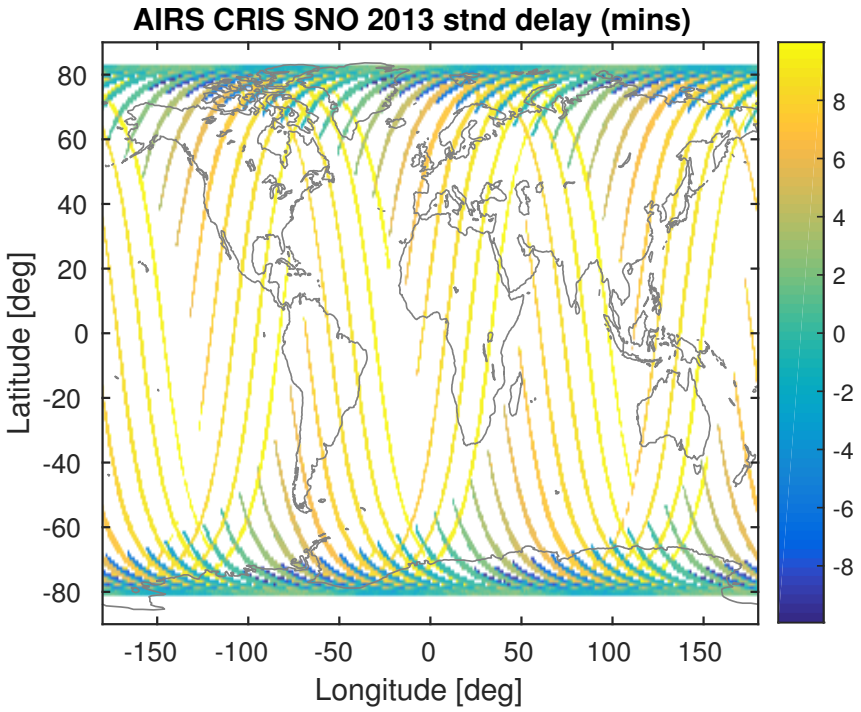

Figure 20: Global distribution of JPL Standard 2013 set, showing delay time in minutes.

channels, with brightness temperatures at the population peak dependent upon the altitude of the weighting function.

For example, figure 24 is a plot of an average spectrum of AIRS and CrIS for a sample of the SNO data. Notice that on this plot the AIRS data are level 1b, and contain some un-filtered bad channels that are not used in the final bias calculations.

With the conversion of AIRS level 1b radiance spectra first to the clean and filled level 1c then to the CrIS spectra grid, allows bias differences to be evaluated across all the CrIS channels for which there are AIRS channels. An example of the mean brightness temperature bias AIRS - CrIS for the long wave (LW) band for all SNO samples in this data set, is shown in figure 25 and for the MW band in figure 26 notice that the standard error is very small.

It is important to note that the original AIRS spectrum of observations include the repaired bad channels and filled gaps and trimmed overlaps, before the spectrum is converted to the CrIS grid, therefore those artifacts

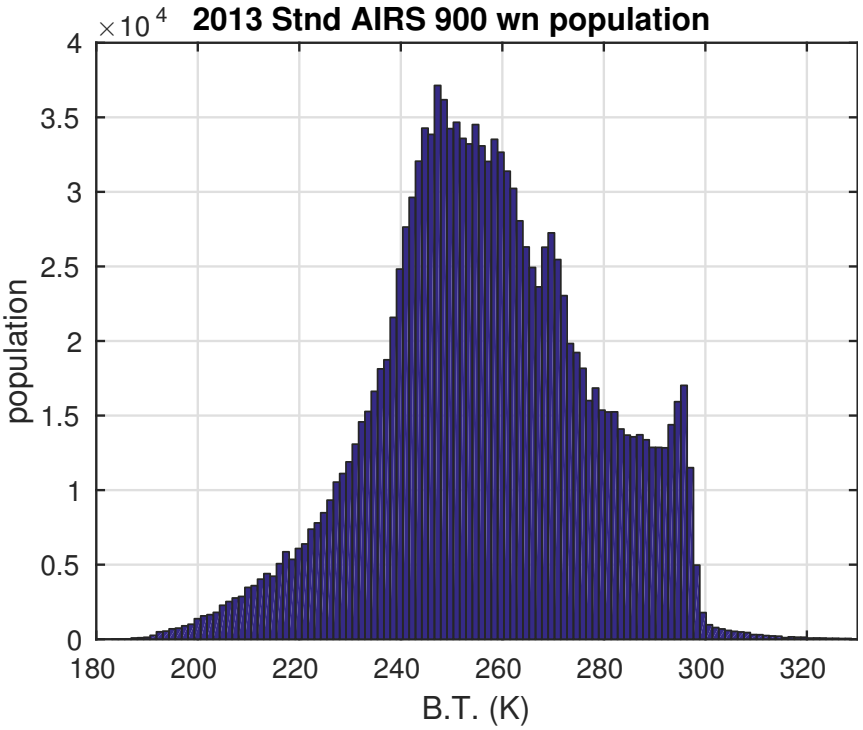

Figure 21: Population distribution of JPL standard 2013 set.

are carried through to these spectral biases. In the final analysis only the original AIRS L1b channels that passed the quality screening used in the L1C processor are selected for evaluation of bias <need reference>. To show just the array module edges see figure 27 in which vertical line markers are used to show the edges. Here one can see the effect of different gain settings for the modules as well as edge effects, and refer to appendix 1.1 for the spectral gaps that are filled by the L1C processor, for example, the region 1046 to 1056 cm^{-1} is a poorly filled gap.

The number of samples in a given month are sufficient to evaluate the temporal trend of the bias, and the result is shown in figure 28 for a window channel. This analysis uses SNO data sets derived from the ASL CCAST CrIS data and AIRS L1C restricted to tropical scenes. The mean bias for this channel for the whole dataset is -0.016 K, which is within uncertainty the same as the previous sets. Note that no spectral calibration has been applied to the AIRS L1b data (pending).

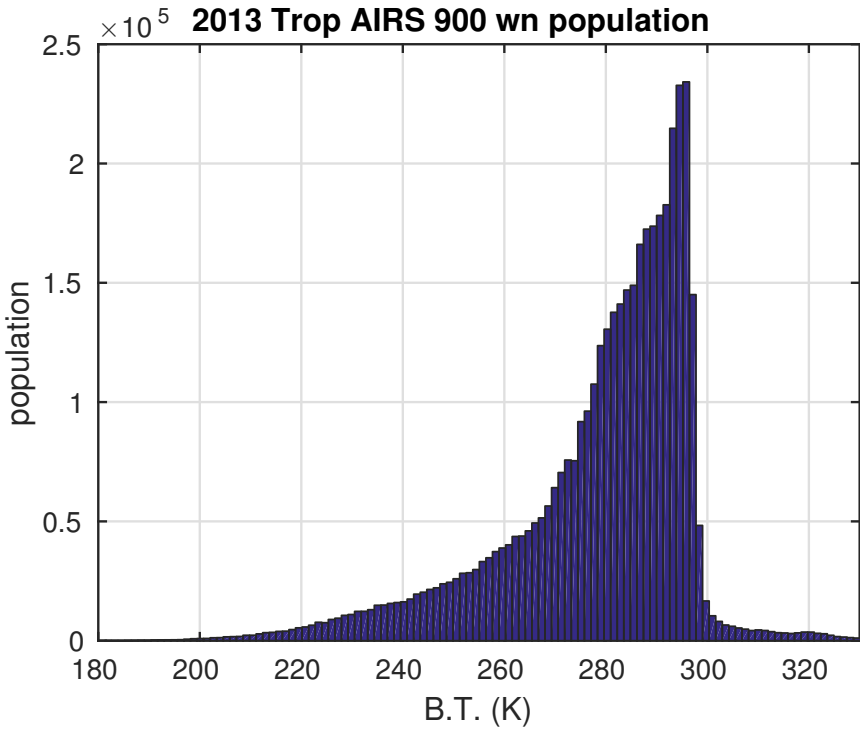

Figure 22: Population distribution of JPL Tropical 2013 subset.

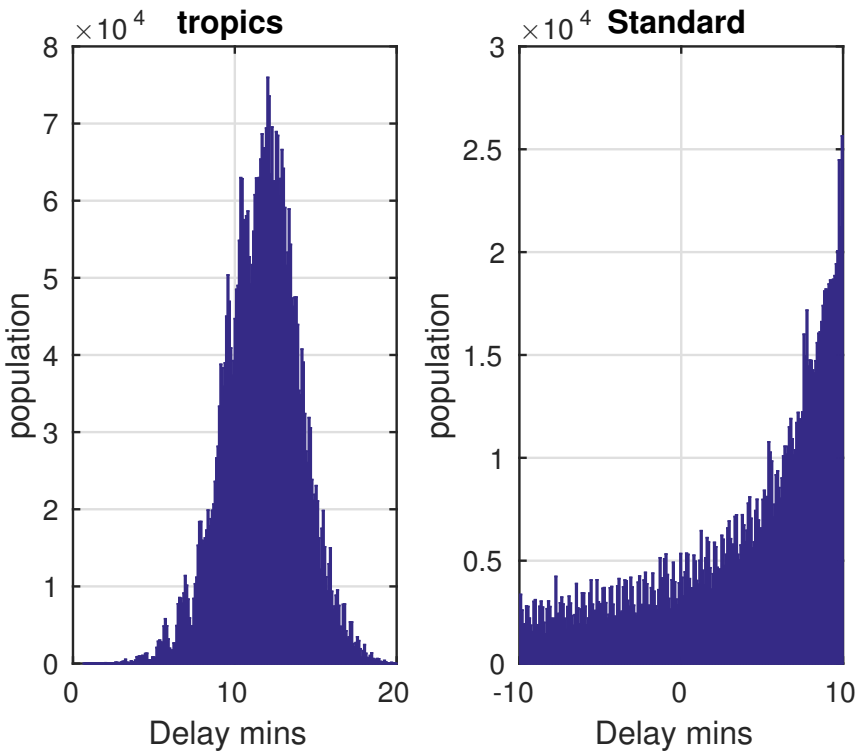

Figure 23: Sensor sample delay (Airs observation time - CrIS observation time).

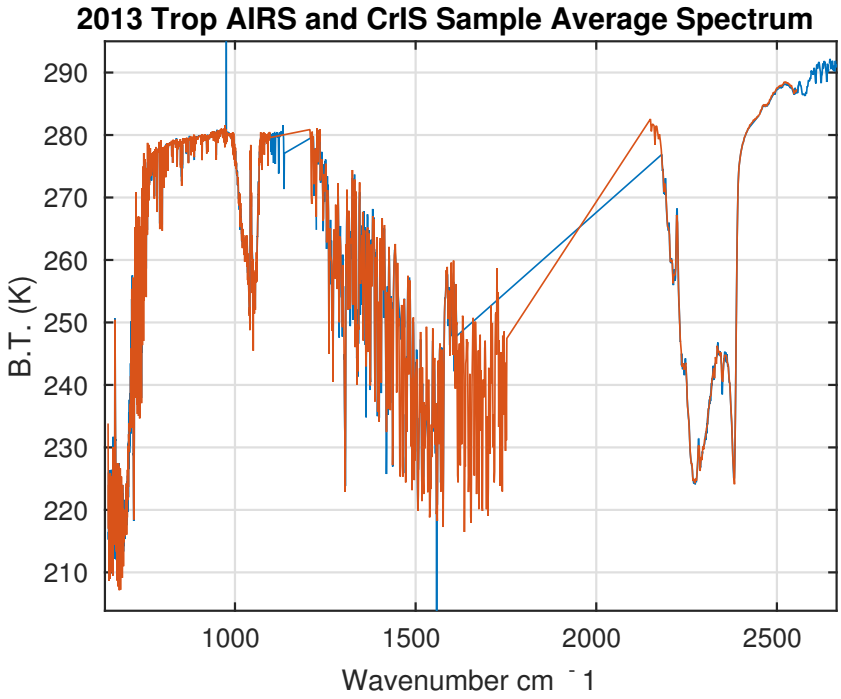

Figure 24: Sample brightness temperature spectrum from the SNO set (Airs blue).

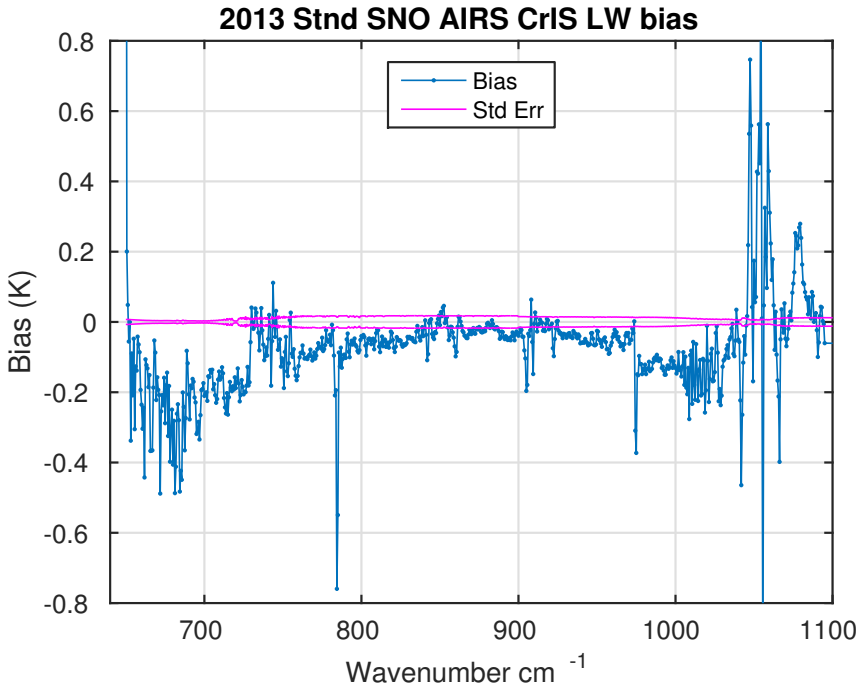

Figure 25: 2013 standard SNO mean sample bias (AIRS - CrIS) in the LW band.

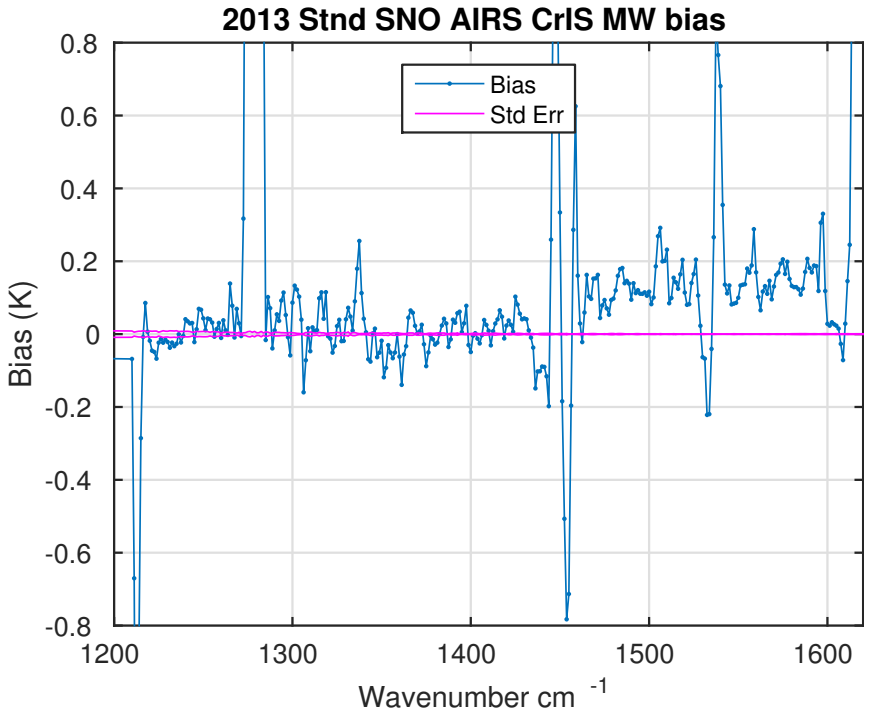

Figure 26: 2013 standard SNO mean sample bias (AIRS - CrIS) in the MW band.

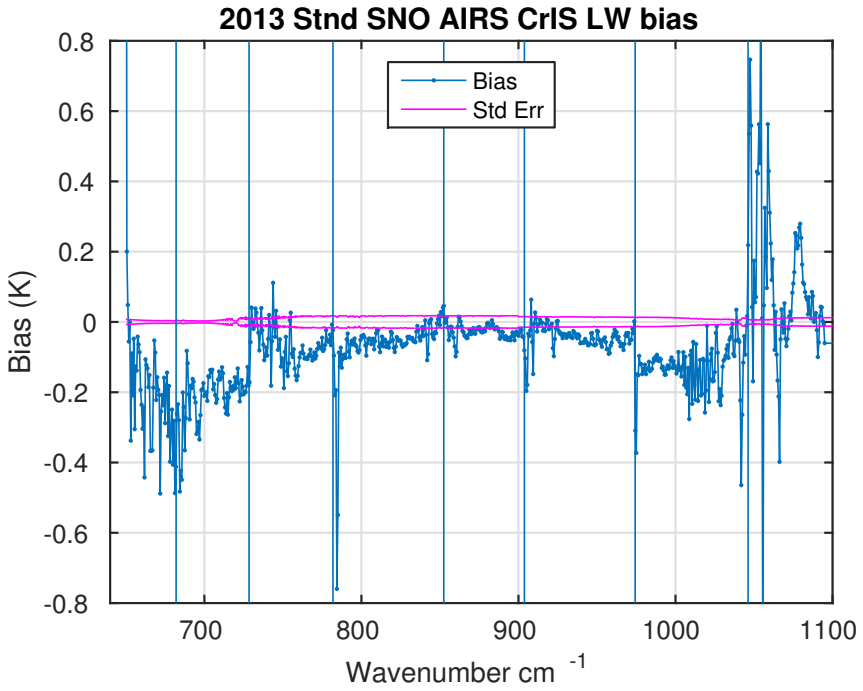

Figure 27: 2013 Tropical SNO mean sample bias (AIRS - CrIS) in the LW band.

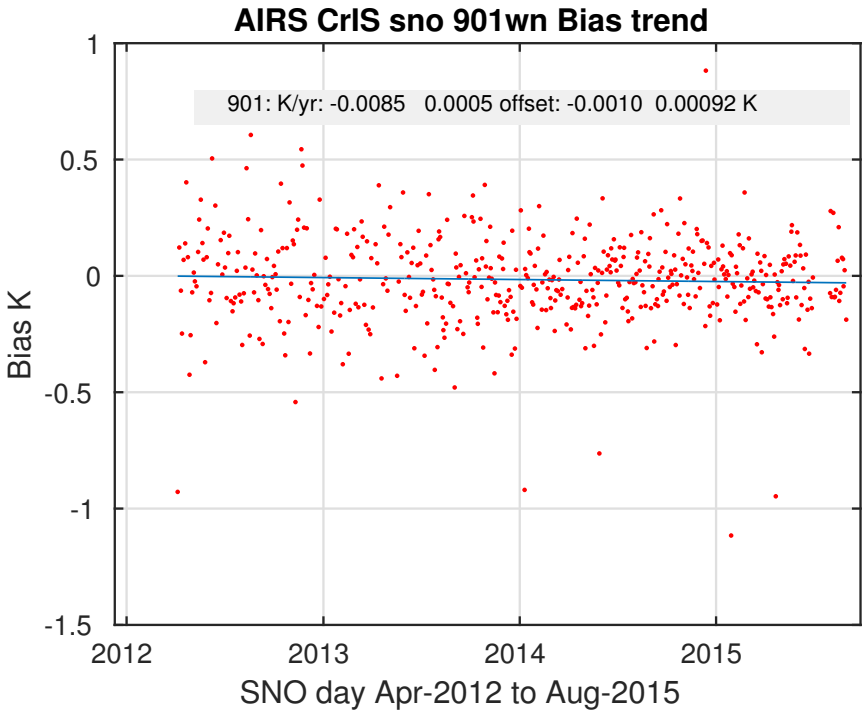

Figure 28: Temporal bias trend (AIRS - CrIS) for a 900 cm-1 channel. (Uncorrected)

6.3 AIRS and IASI SNOs

The AIRS and IASI SNOs are restricted to the near-polar latitudes similar to the CrIS and IASI SNOs discussed previously. The criteria for selection based upon spatial and temporal separation is the same as for CrIS and IASI SNOs. The complete data set consists approximately 434,000 observation pairs over the time period 2011-Jan to 2014-Mar.

The deconvolution of IASI onto the AIRS SRFs is less reliable than the previous two conversions because of the resolution differences, and will not normally be performed for trending analysis. As seen in the following figure, it is also rather noisy from channel to channel. The brightness temperature bias AIRS - IASI for the LW band using all samples is shown in figure 29 which includes all the bad and filled AIRS channels, after processing to level 1c. Nevertheless, a general trend of the bias can be observed across the LW band and between modules.

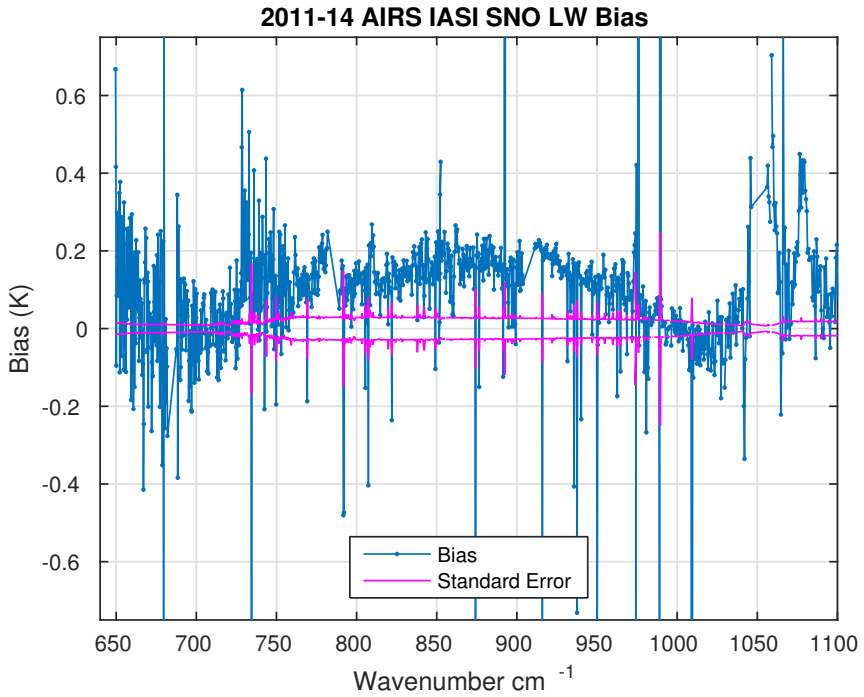

Figure 29: AIRS IASI SNO bias for the LW band.

For completeness, the variation of bias as a function of scene brightness for the window channel at 900 cm^{-1} is shown in figure 30 notice that most

observations are around 250 K because of the polar coverage.

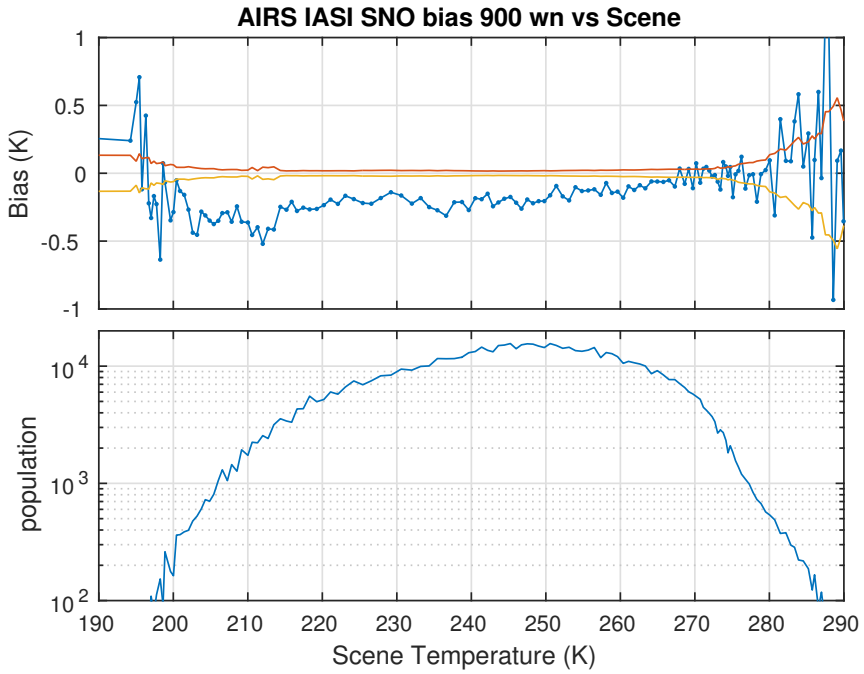

Figure 30: AIRS IASI SNO bias for the 900 cm window channel as a function of scene.

6.4 AIRS and IASI on the common CrIS grid

The bias between the sensor pairs AIRS and CrIS, AIRS and IASI, IASI and CrIS, is evaluated using the SNO sets as described above, but now using the CrIS spectral grid as the common grid. Note that after the change of resolution of CrIS, the LW band remains the same, and the level one procesing can be performed so that the standard resolution or the new resolution may be utilized. In any case, as pointed out previously, the deconvoltion and translation between sensors is numerically better if it goes from a higher resolution to lower resolution system.

The bias for each of the three pairs of sensor SNO sets is shown in figure 31 for the LW band. The upper panel shows the airs compared to CrIS and IASI and the lower panel CrIS compare to IASI. In all cases the AIRS and IASI spectra have been converted to the CrIS grid. The standard errors are not plotted for clarity, but have numerical values the same as reported in the

preceding sections. Note that by eye, the CrIS - IASI bias follows the double difference from the upper panel. As before, the AIRS spectra retain some of the artifacts from the L1C processing, such as filled gaps and repaired channels.

The same results are plotted in figure 32 for the middle band (MW) region.

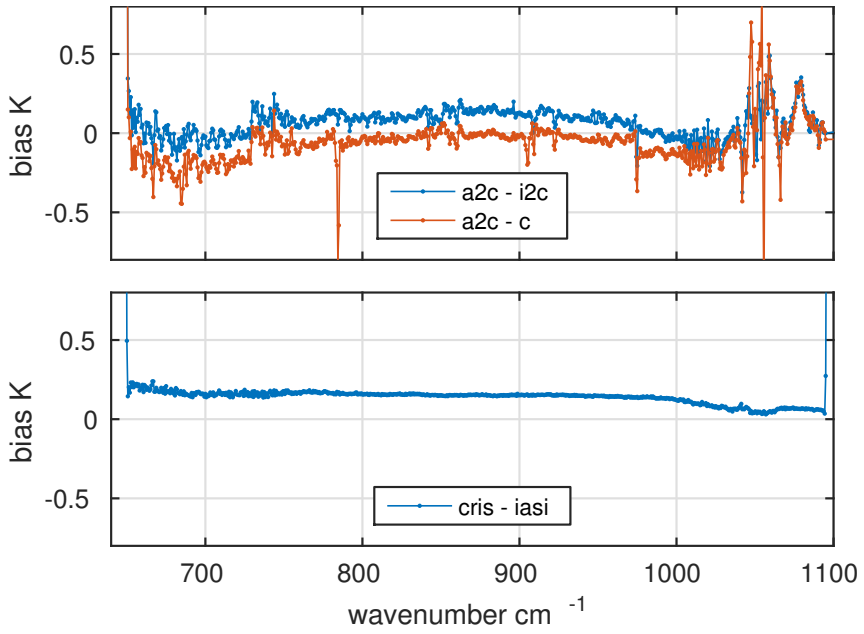

Figure 31: Combined plot all biases referenced to the CrIS grid. Upper panel: AIRS - IASI (blue) AIRS - CrIS (red), lower panel: CrIS - IASI. LW band

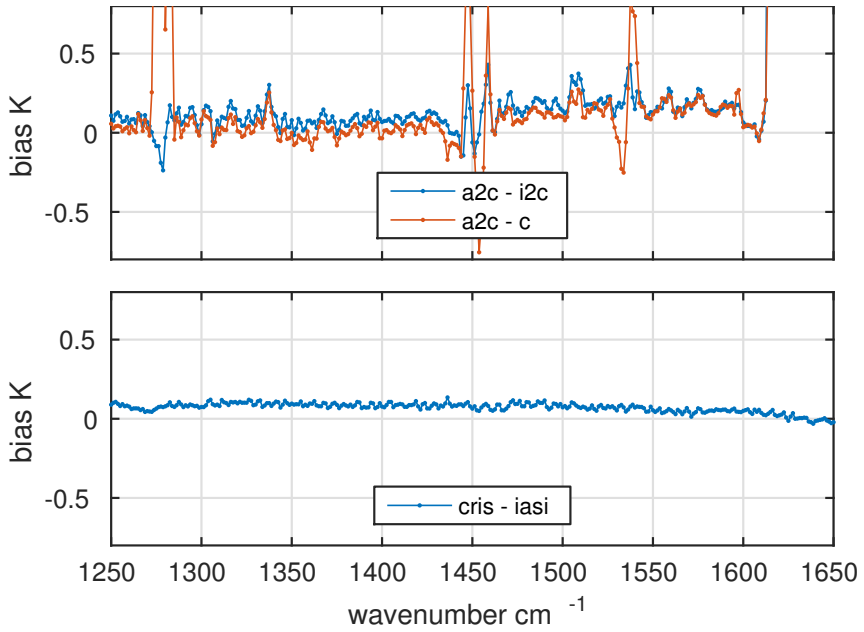

Figure 32: Combined plot all biases referenced to the CrIS grid. Upper panel: AIRS - IASI (blue) AIRS - CrIS (red), lower panel: CrIS - IASI. MW band

7 Conclusions

The methods described in this paper provide a quantitative means to determine the bias, expressed in terms of brightness temperature, between different sensors across a relatively large spectral range. It does not, and can not, determine which sensor is the more accurate, but can provide clues as to how a given sensor is behaving when it exhibits the same bias characteristics against two independent sensors. In the case of AIRS, for example, there are distinct changes between some of the different detector modules.

There are a few points to bear in mind when interpreting the results and some limitations of the method, which can be divided into intrinsic and sampling effects. In the deconvolution and translation to a different spectral grid, there tends to be ringing at the boundaries, which is mathematically inevitable, so caution should be made when comparing the first 5 or so channels at the boundaries of the full spectral range. The conversion is perfect where the the spectrum is flat or the nominal resolution perfectly captures the underlying spectral features. Examination of the residuals in the valida-

tion plots above, reveal these attributes, however they do not significantly add to the bias. In all cases the conversion to the interferometric ILS spectral wavenumber is followed by Hamming apodization.

In respect of sampling effects, the method would give a perfect analysis of sensor bias if either the Earth scenes were perfectly spatially uniform and static, or the fields of view of the different sensors perfectly matched the same Earth scene at the same time. Furthermore, the results must be interpreted in the context of the dynamic range of the scenes, as illustrated in the figures showing scene dependent bias. Although the sampling is not perfect and scenes not uniform, there are sufficiently large numbers of SNO pairs available that statistical variations can be well characterized and mean bias is statistically significant. This is also illustrated in the scene dependent bias plots. In general, toward the hot and cold extreme scenes the sampling becomes limited, and especially in the hot scenes, the sampling is only over land during the day, e.g. figure 20, for which there is a significant time delay between the two sensors. There is clearly some advantage in restricting the SNOs to clear tropical ocean views, but then the dynamic range would be limited, at least for the window channels.

One application of the method described here is for the creation of a long term climate radiance record from multiple sensors, that have suitable operational overlap. The best way to create such a record is to match the bias for each spectral channel on the common grid over the longest possible time period and dynamic range of the operational overlap. If the bias for this period is constant then a simple adjustment of the radiance based on the bias reported here can be applied. If there is no independent or corroborating measurement to alter the weight of each sensor, then equal weights are applied and the average bias would be applied to each sensor to create the most likely radiance on the common grid.

8 Further work

TBD

9 Acronyms:

- AIRS: Atmospheric Infra-Red Sounder.
- CRIS: Cross Track Infrared Sounder.
- ECV: Essential Climate Variables.

- GCOS: Glocal climate Observing System.
- IASI: Infra-red Atmospheric Sounding Interferometer.
- ILS: Instrument Line Shape.
- LBL: Line-by-line.
- SRF: Spectral Response Function.
- TOA: Top of Atmosphere.
- UMBC: University of Maryland Baltimore County.
- WMO: World Meteorological Organisation

10 References:

References

[1] Wielicki et al., , BAMS 2013 DOI:10.1175/BAMS-D-12-00149.1

[2] $https://www.ipcc.ch/publications_and_data/ar4/wg1/en/ch3.html$

[3] $http://www.wmo.int/pages/prog/gcos/index.php?name=ClimateObservationNeeds$

[4] Strow et al. Pre-launch Spectral Calibration of the Atmospheric Infrared Sounder. IEEE trans. Geosci. remote sens, vol 41,(2) 2003, pp 274. DOI: 10.1109/TGRS.2002.808245

[5] Aumann, H.H., and Miller, Chris, "Atmospheric Infrared Sounder (AIRS) on the Earth Observing System", SPIE Vol.2583, 32-343, 1995.

[6] $http://www.jpss.noaa.gov/cris.html$

[7] Tobin. D. et al. Suomi-NPP CrIS radiometric calibration uncertainty. J. Geophys Re. Atmos. 118 (2013) pp 10,589 - 10,600. doi: 10.1002/jgrd.50809

[8] $http://www.eumetsat.int/website/home/Satellites/CurrentSatellites/Metop/MetopDesign/I$

[9] Chalon G, Cayla F, Diebel D. 2001. 'IASI: an advanced sounder for operational meteorology'. Proceedings of the 52nd Congress of IAF, Toulouse, France, 1–5 October 2001.

PDO: Minobe, S. 1997: A 50-70 year climatic oscillation over the North Pacific and North America. Geophysical Research Letters, Vol 24, pp 683-686.

Bond, N.A. and D.E. Harrison (2000): The Pacific Decadal Oscillation, air-sea interaction and central north Pacific winter atmospheric regimes. Geophys. Res. Lett., 27(5), 731-734.

AMOC: Trenberth, K.E. and D.J. Shea (2006): Atlantic hurricanes and natural variability in 2005. Geophysical Research Letters 33, L12704, 10.1029/2006GL026894 [pdf]

Schlesinger, M.E. and Navin Ramankutty (1994): An oscillation in the global climate system of period 65-70 years. Nature, 367, Issue 6465, pp. 723-726, DOI: 10.1038/367723a0

ENSO: The 1990–1995 El Niño-Southern Oscillation Event: Longest on Record Kevin E. Trenberth andTimothy J. Hoar. Geophysical Research Letters Volume 23, Issue 1, pages 57–60, 1 January 1996.

Leetmaa, A. 1999: The first El Niño observed and forecasted from start to finish. Bull. Am. Met. Soc., 80, 111-112.

ECVs http://www.wmo.int/pages/prog/gcos/

11 Appendices

11.1 AIRS L1C filled gaps

681.99, 687.60
781.88, 789.26
903.78, 911.23
1046.20, 1056.07
1136.63, 1216.97
1272.59, 1284.35
1443.07, 1460.27
1527.00, 1541.10
1613.86, 2181.49
2557.41 ,2558.53